

SUPPORTING INFORMATION

Quantitative Assessment of the Dynamic Modification of Lipid-DNA Probes on Live Cell Membranes

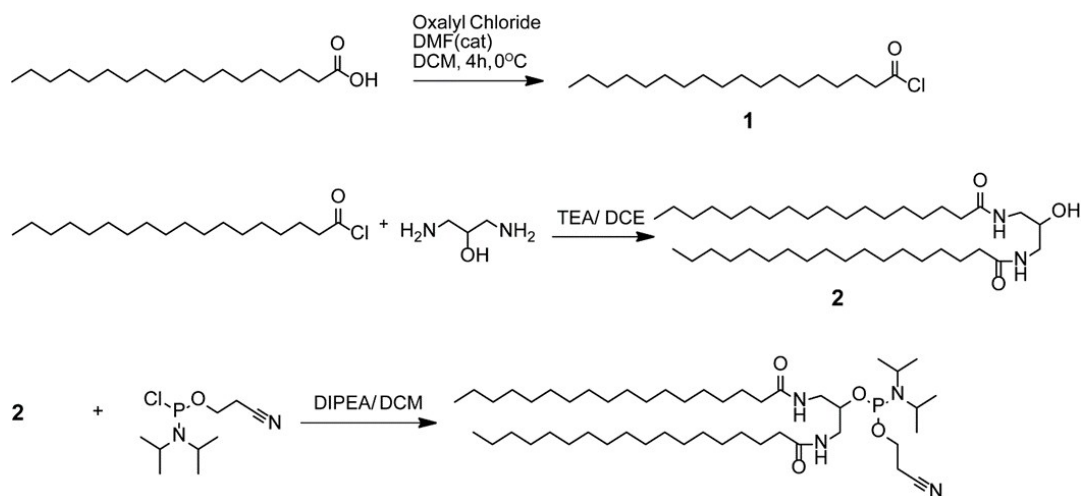
Yousef Bagheri, Sara Chedid, Fatemeh Shafiei, Bin Zhao*, and Mingxu You*

Department of Chemistry, University of Massachusetts, Amherst, MA 01003, USA.

* Correspondence: mingxuyou@umass.edu ; bzhao@umass.edu

1. SUPPLEMENTARY METHODS

Lipid synthesis. Two-carbon-chain lipids were synthesized following a previously described protocol (Scheme 1).¹



Synthesis of 18:0-18:0 phosphoramidite. Briefly, stearyl chloride was first synthesized from stearic acid with the addition of oxalyl chloride and catalytic amount of dimethylformamide (DMF). Here, stearic acid (400 mg, 1.36 mmol) was dissolved in ice-cooled anhydrous dichloromethane (DCM). Oxalyl chloride (344 mg, 2.72 mmol) in 2 ml DCM was mixed with catalytic amount of DMF and added into the stearic acid solution dropwise in 5 min. The reaction mixture was stirred at 0°C for 2 h. After removing the excess oxalyl chloride under the vacuum, the product stearyl chloride was directly used for next step.

In the next step, the stearyl chloride (4.0 g, 13.14 mmol) solution in dichloroethane (30 mL) was added into 1,3-diamino-2-dihydroxypropane (0.589 g, 5.54 mmol) in the presence of trimethylamine (1.706 g, 13.14 mmol). Reaction was continued at room temperature for 2 h and then at 70°C for overnight. After cooling to room temperature, solid was separated through filtration and washed with cold DCM, methanol, 5% sodium bicarbonate and acetone. The crude product was then purified by column chromatography to afford 3.1 g (75%) as white solid.

The intermediate product (2.19 g, 3.2 mmol) was dissolved in ice-cooled DCM (50 ml) along with diisopropylethylamine (0.91g, 7.04 mmol). A solution of 2-cyanoethyl-N,N'-diisopropylchlorophosphoramidite (1 g, 4.2 mmol) in DCM (5 ml) was added dropwise into this solution and stirred at room temperature for 1 h and then 60°C for 2 h. The final product was purified by precipitation from acetone and column chromatography to yield 1.2 g (44%) of white solid.

¹H-NMR (400 MHz, CDCl₃): δ (ppm) 0.9 (t, 6H), 1.2-1.4 (m, 72H), 1.6 (m, 4H), 2.2 (t, 4H), 2.6 (t, 2H), 2.8-3.1 (m, 2H), 3.6 (m, 2H), 3.8 (m, 2H), 3.9 (m, 2H). ¹³C NMR (100 MHz, CDCl₃): δ (ppm) 174.4, 118.16, 70.70, 58.18, 43.11, 40.37, 36.40, 30.01, 24.32, 21.13, 14.41. ³¹P NMR (162 MHz, CDCl₃): δ (ppm) 147. ESI-MS: (C₄₈H₉₅N₄O₄P+Na⁺) calculated, 846.29; found, 845.6390.

Synthesis of 16:0-16:0 phosphoramidite. 16:0-16:0 phosphoramidite was synthesized following a similar procedure as that of 18:0-18:0 phosphoramidite. Briefly, palmitoyl chloride (3.63g, 13.14 mmol) was dissolved in 40 ml of dichloroethane and added to 1,3-diamino-2-dihydroxypropane (0.589 g, 5.54 mmol) in the presence of trimethylamine (1.706 g, 13.14 mmol). Reaction was continued at room temperature for 2 h and then at 70°C for overnight. Mixture was cooled to room temperature and solid was separated by filtration and washed with cold DCM, methanol, 5% sodium bicarbonate and acetone. Product was further purified by column chromatography to afford 2.57g (69 %) as white solid.

The synthesized lipid (2.10g, 3.2 mmol) was dissolved in 50 ml of ice-cold DCM in the presence of diisopropylethylamine (0.91g, 7.04 mmol). A solution of 2-cyanoethyl-N,N'-diisopropylchlorophosphoramidite (1 g, 4.2 mmol) in DCM (5 ml) was added dropwise into this solution and stirred at room temperature for 1 h and then 60°C for 2 h. The final product was purified by precipitation from acetone and column chromatography to afford 1.37g (56% yield) as white solid.

¹H-NMR (400 MHz, CDCl₃): δ (ppm) 0.9 (t, 6H), 1.2-1.4 (m, 64H), 1.6 (m, 4H), 2.2 (t, 4H), 2.6 (t, 2H), 2.8-3.1 (m, 2H), 3.6 (m, 2H), 3.8 (m, 2H), 3.9 (m, 2H). ¹³C NMR (100 MHz, CDCl₃): δ (ppm) 174.68, 118.45, 71.14, 58.42, 43.50, 40.89, 37.05, 32.22, 26.51, 21.42, 14.23. ³¹P NMR (162 MHz, CDCl₃): δ (ppm) 148. ESI-MS: (C₄₄H₈₇N₄O₄P+Na⁺) calculated, 789.65; found, 788.5922.

Synthesis of 18:1-18:1 phosphoramidite. 5 g (16.64 mmol) of oleoyl chloride was dissolved in 50 ml of DCM and added into 1,3-diamino-2-dihydroxypropane (0.746g, 7 mmol) in the presence of trimethylamine (2.16 g, 16.64mmol). Reaction was completed following 2 h mixing at room temperature and overnight at 70°C. The mixture was cooled down and DCM was evaporated under vacuum. The product was purified with column chromatography to afford 3.71g (72%) colorless oil.

The solution of synthesized lipid (2.0 g, 2.94 mmol) and diisopropylethylamine (0.836g, 6.47 mmol) was prepared in ice-cold DCM. Solution of 2-cyanoethyl-N,N'-diisopropylchlorophosphoramidite (0.920g, 3.85) in DCM (5 ml) was added dropwise into this solution and reaction was completed by mixing for 1 h at room temperature and 2 hours at 60°C. The final purified product as a pale-yellow oil (1.54g, 64% yield) was obtained by column chromatography.

¹H-NMR (400 MHz, CDCl₃): δ (ppm) 0.9 (t,6H), 1.2-1.5 (m, 44H), 1.6 (m, 4H), 2.1 (m, 8H), 2.4 (t, 4H), 3.1 (m, 2H), 3.4 (d, 4H), 5.4 (m, 4H). ¹³C NMR (100 MHz, CDCl₃): δ (ppm) 174.99, 129.89, 118.3, 77.36, 69.90, 57.18, 40.62, 36.58, 32.44, 29.32, 27.31, 22.16, 14.62. ³¹P NMR (162MHz, CDCl₃): δ (ppm) 147. ESI-MS: (C₄₈H₉₁N₄O₄P+Na⁺) calculated, 842.25; found, 842.6072.

Synthesis of lipid-DNA conjugation. Using a standard phosphoramidite chemistry, dialkylglycerol phosphoramidite was coupled with 5'-OH oligonucleotides on controlled pore glass. More specifically, 500 uL of dialkylglycerol phosphoramidite (200 mM) and 1 mL 5-(ethylthio)-1H-tetrazole (250 mM) were dissolved in DCM, loaded into a syringe, and mixed for 15 min with 200 nmol of DNA on beads in a conjugation column. Care must be taken because this process is highly moisture sensitive and even small amount of moisture drops the efficiency significantly. Using Amidation reaction for 18.1-modified DNA as an example, 20 μmol oleoyl chloride was further reacted with 200 nmol amine-modified

oligonucleotides on the beads in the presence of 20 μmol trimethylamine. The mixture was shaken at room temperature overnight. Lipid-modified DNA was then cleaved from the beads and purified by reversed phase HPLC using a C4 column with 100 mM triethylammonium acetate buffer (pH 7.5) and acetonitrile (0 – 30 min, 10 – 100%) as an eluent.

Measurement of lipid-DNA hydrophobicity. The hydrophobicity of the purified lipid-DNA conjugates were measured by analyzing their retention time in reversed phase HPLC^{2,3}. A constant 95% A (water + 0.1% TEAA) and 5% B (ACN) mixture was used as the eluent and C₄ column as a stationary phase. Distribution constant and hydrophobicity can be further calculated based on the obtained retention time of each lipid-DNA conjugate as explained below.

The distribution constant (K_c) is defined as the ratio of the activity (α) of the lipid-DNA conjugates (LD) between the stationary phase and mobile phase. At low concentration, it is a safe approximation to replace the activity with the concentration of the lipid-DNA conjugates (equation 1).

$$\begin{array}{c}
 \text{LD}_m \xrightleftharpoons{K_c} \text{LD}_s \\
 K_c = \frac{(\alpha_{LD})_s C_s}{(\alpha_{LD})_m C_m} \cong \frac{C_s}{C_m}
 \end{array} \quad (1)$$

The retention factor (k_c) can be derived from the distribution constant according to equation 2, in which V_s and V_m are the stationary and mobile phase volume, respectively. V_s and V_m are two characteristics that depend on the column used in the experiment.

$$k_c = \frac{K_c \cdot V_s}{V_m} \quad (2)$$

The retention factor can be measured from the retention time following the equation 3 in which f_m is the fraction of LD in the mobile phase.

$$k_c = \frac{1 - f_m}{f_m} \quad (3)$$

Since a constant flow rate was used, we can determine the retention factor based on the retention time.

$$f_m = \frac{t_m}{t_r} \quad (4)$$

$$k_c = \frac{1 - \frac{t_m}{t_r}}{\frac{t_m}{t_r}} = \frac{t_r - t_m}{t_m}$$

$$K_c = \frac{V_m}{V_s} \left(\frac{t_r - t_m}{t_m} \right)$$

t_r = retention time, t_m = void time

Finally, the hydrophobicity ($\log p$) can be measured using the following equation.

$$\log p = \log K_c = \log \left(\frac{V_m}{V_s} \left(\frac{t_r - t_m}{t_m} \right) \right)$$

MALDI characterization. To characterize the as-prepared lipid-DNA conjugates, first, saturated amount of 3-hydroxypicolinic acid was prepared in a 1:1 solution of acetonitrile: water (5% ammonium citrate and 0.1% trifluoroacetic acid). Then, 1 μ L of HPLC-purified DNA (10–30 μ M) was mixed with equal volume of matrix and deposited on a ground steel MALDI plate (Bruker, Germany). Solvents were removed by air-drying prior to the mass determination. Measurement was performed using a Bruker microflex device.

Total internal reflection fluorescence (TIRF) measurement. A motorized inverted microscope ECLIPSE Ti2-E, equipped with ORCA-Flash 4.0 sCMOS camera and TIRF module, was used to monitor probe dynamics on cell membranes. Imaging data was collected with an Apo TIRF 60x oil DIC N2 objective (NA 1.49) and was analyzed using NIS-Elements software. To minimize the photobleaching of lipid-DNA probes on the cell membranes, an Atto488-modified cholesterol-DNA probe was used in this TIRF measurement. HeLa cells were chosen as the example. These cells were first incubated with 20 nM probes for 30 min and then the dynamic membrane motion of the probes were monitored at the single-molecule level at room temperature.

Cell membrane probe density measurement. A supported lipid monolayer was used to measure the probe density on the cell membrane^{4,5}. In this method, different ratios of lipid-DNA probes and the soybean polar extract were mixed and incubated at 4°C for overnight. Afterwards, 10 μ L mixture was placed on a Teflon-coated microscope glass coverslide, dried under the airflow to remove chloroform, and then rehydrated with 5 μ L HEPES buffer. The obtained probe-incorporated lipid monolayers were then imaged with a confocal microscope using the same imaging parameters as that during the cellular studies. The surface area of the monolayer and the probe density per unit surface area was then calculated. A calibration curve was established between the probe densities and the corresponding fluorescence intensities (Figure S3d). This calibration curve was further used to determine the probe densities on live cell membranes.

Determination of the probe internalization rate constant (k_{int}). Our results indicated a first-order reaction model of the internalization process (Figure S12c), which is consistent with some previous studies⁶⁻⁹. These lipid-DNA probes get internalized by first interacting with cell membranes. Therefore, the membrane surface can be considered as a substrate of the endocytosis or internalization. Then the internalization kinetics can be considered to depend on the probe densities on the membrane:

$$\frac{d[LD]_i}{dt} = k_{int}[LD]_m$$

Where $[LD]_i$ and $[LD]_m$ is the number of the probes inside cells or on the membrane, and k_{int} is the internalization rate constant. For this equation to be valid, it is critical that the probe removal with the processes such as exocytosis, degradation and fluorescence quenching is minimal.

$$\frac{d[LD]_i}{[LD]_m} = k_{int} dt$$

Considering that during the initial time of internalization, the probe density on the cell membrane is approximately constant ($\frac{d[LD]_m}{dt} \approx 0$), thus the integration of the above equation will be as follows.

$$\frac{1}{[LD]_m} \int_{[LD]_{i_0}}^{[LD]_i} d[LD]_i = k_{int} \int_{t_0}^t dt$$

Which will be solved to give:

$$\frac{[LD]_i - [LD]_{i_0}}{[LD]_m} = k_{int}(t - t_0)$$

Since at the initial time (t_0), the inserted probe is zero ($[LD]_{i_0} = 0$), then

$$\frac{[LD]_i}{[LD]_m} = k_{int} t$$

It is worth mentioning that the third equation can have an exact solution if $\frac{d[LD]_m}{dt} = 0$. However, even in the case that the membrane signal changes for a small extent, this will be still a valid approximation if

the measurement time is short⁶. By plotting the $\frac{[LD]_i}{[LD]_m}$ versus the time, instead of using the probe concentration in the solution^{6,7}, the internalization rate constant will be derived (Figure S12d).

In addition to the relatively steady membrane probe density, for this calculation to be valid, it is necessary that the probe is not degraded in lysosome, or late endosome. Furthermore, the exocytosis as a method that cells remove the internalized material, should be minimized in the measurement windows. Finally, since FAM is a pH-sensitive dye and it gets quenched at lower pH, care must be taken to minimize this effect. Considering all these reasons, we measured the initial rate constant rather than overall rate constant that can be dramatically affected by these factors.

2. SUPPLEMENTARY TABLES

Table S1. DNA sequences used in this study

Name	Sequence (5'–3')
20 nt	Lipid -TGATGTGGTGTGTGAGAGAG- FAM
40 nt	Lipid -AGGGTGAGTGAGATGTGAGTGAGGAGTGGAGAGAAGTAGT- FAM
60 nt	Lipid -CTCCCTACCATCACCTCCACACAACCTACCACCCACATCCCCTACTTCTCTC CACTTTTA- FAM
80 nt	Lipid -CTCCCTACCATCACCTCCACACAACCTACCACCCACATCCCCTACTTCT CTCCACTTTTCACTCACATTTCACTCACCCCT- FAM
20 nt-CS	CTCTCTCACACACCACATCA
80 nt-CS	AGGGTGAGTGAAATGTGAGTGAAAAGTGGAGAGAAGTAGTGGGATGTGGGTGGTA GTTGTGTGGAGGTGATGGTAGGGAG
77 nt-Cy5	Lipid -CCCGTGAAATACCGCACAGATGCGTTTGTATAAATGTTTTTTTCATTTATAC TTAAGAGCGCCACGTAGCCCAGC- Cy5

Table S2. The calculated and MALDI-based experimental molecular weight values for each 20 nt lipid-DNA probe

Type of lipid (20 nt DNA)	Calculated molecular weight [M+H] ⁺	Measured molecular weight [M+H] ⁺
18:0	7125	7173 ± 42
16:0-16:0	7434	7440 ± 12
18:0-18:0	7493	7501 ± 07
16:0-18:1	7992	7991 ± 41
18:1	7254	7243 ± 13
18:1-18:1	7604	7626 ± 61
Cholesterol	7601	7582 ± 21

Table S3. Lipid-DNA probe insertion kinetics onto MDCK cell membranes

Type of lipid	k_{in} (s ⁻¹)	T _{0.5} (min)	T _{0.9} (min)	k_{in} (s ⁻¹) (37°C)	T _{0.5} (min) (37°C)	T _{0.9} (min) (37°C)
Cholesterol	0.033 ± 0.001	1.6	8.2	0.086 ± 0.002	1.3	2.9
18:0	0.032 ± 0.002	1.7	7.1	0.061 ± 0.001	2.5	4.2
18:1	0.024 ± 0.001	3.1	8.5	0.065 ± 0.003	1.7	3.4
16:0-16:0	0.019 ± 0.002	3.4	19.2	0.072 ± 0.001	7.5	20.1
16:0-18:1	0.023 ± 0.002	2.8	30.7	0.053 ± 0.002	4.4	16.4
18:0-18:0	0.019 ± 0.001	8.7	31.3	0.092 ± 0.001	9.1	17.1
18:1-18:1	0.009 ± 0.003	3.8	24.5	0.079 ± 0.003	6.7	17.5

T_{0.5} and T_{0.9}: the time that 50% and 90% of the probe was inserted onto MDCK cell membranes
 k_{in} : cell membrane insertion rate constant of the probes

Table S4. Critical aggregation concentration values of different lipid-DNA probes

Type of lipid-DNA probe	Critical aggregation concentration (μM)	k_{in} (s ⁻¹)
Cholesterol (SS)	2.2	0.033 ± 0.001
18:0 (SS)	>15	0.032 ± 0.002
18:1 (SS)	>15	0.024 ± 0.001
16:0-16:0 (SS)	0.90	0.019 ± 0.002
16:0-18:1 (SS)	0.86	0.023 ± 0.002
18:0-18:0 (SS)	0.86	0.019 ± 0.001
18:1-18:1 (SS)	0.93	0.009 ± 0.003
Cholesterol (SS 40 nt)	5.2	-
Cholesterol (SS 60 nt)	10.2	-
Cholesterol (SS 80 nt)	>15	-
Cholesterol (DS)	2.7	-
18:0-18:0 (DS)	1.4	-

SS: single-stranded 20 nt DNA;

DS: double-stranded 20 nt DNA duplexes

Table S5. Insertion efficiency of different probes on the MDCK cell membrane

Type of lipid	Probe/ nm ² (25°C, SS)	Probe/ nm ² (37°C, SS)	Probe/ nm ² (25°C, DS)
Cholesterol	0.20 ± 0.004	0.10 ± 0.009	0.12 ± 0.010
18:0	0.12 ± 0.003	0.06 ± 0.008	0.10 ± 0.008
18:0-18:0	0.14 ± 0.009	0.07 ± 0.008	0.14 ± 0.008
16:0-16:0	0.13 ± 0.004	0.06 ± 0.008	0.11 ± 0.007
16:0-18:1	0.03 ± 0.003	0.03 ± 0.005	0.04 ± 0.005
18:1	0.02 ± 0.003	0.02 ± 0.005	0.02 ± 0.004
18:1-18:1	0.02 ± 0.009	0.02 ± 0.006	0.02 ± 0.006

SS: single-stranded 20 nt DNA; DS: double-stranded 20 nt DNA duplex

Table S6. Cell membrane diffusion coefficient of lipid-DNA probes as measured with fluorescence recovery after photobleaching

Type of lipid-DNA probe	Beam radius (μm)	T _{0.5} (ms)	D (μm ² /s)
18:0 (SS)	2.56	36958	0.044 ± 0.004
Cholesterol (SS)	2.56	53195	0.031 ± 0.003
18:1 (SS)	2.56	55195	0.029 ± 0.006
16:0-16:0 (SS)	2.56	63886	0.026 ± 0.003
18:0-18:0 (SS)	2.56	75460	0.022 ± 0.001
16:0-18:1 (SS)	2.56	89800	0.018 ± 0.002
18:1-18:1 (SS)	2.56	93294	0.017 ± 0.005
Cholesterol (DS)	2.56	54389	0.030 ± 0.004
18:0-18:0 (DS)	2.56	77885	0.021 ± 0.006
18:0 (DS)	2.56	42525	0.039 ± 0.003
Cholesterol (80 nt)	2.56	81527	0.020 ± 0.005

SS: single-stranded 20 nt DNA; DS: double-stranded 20 nt DNA duplexes

80 nt: single-stranded 80 nt DNA

3. SUPPLEMENTARY FIGURES

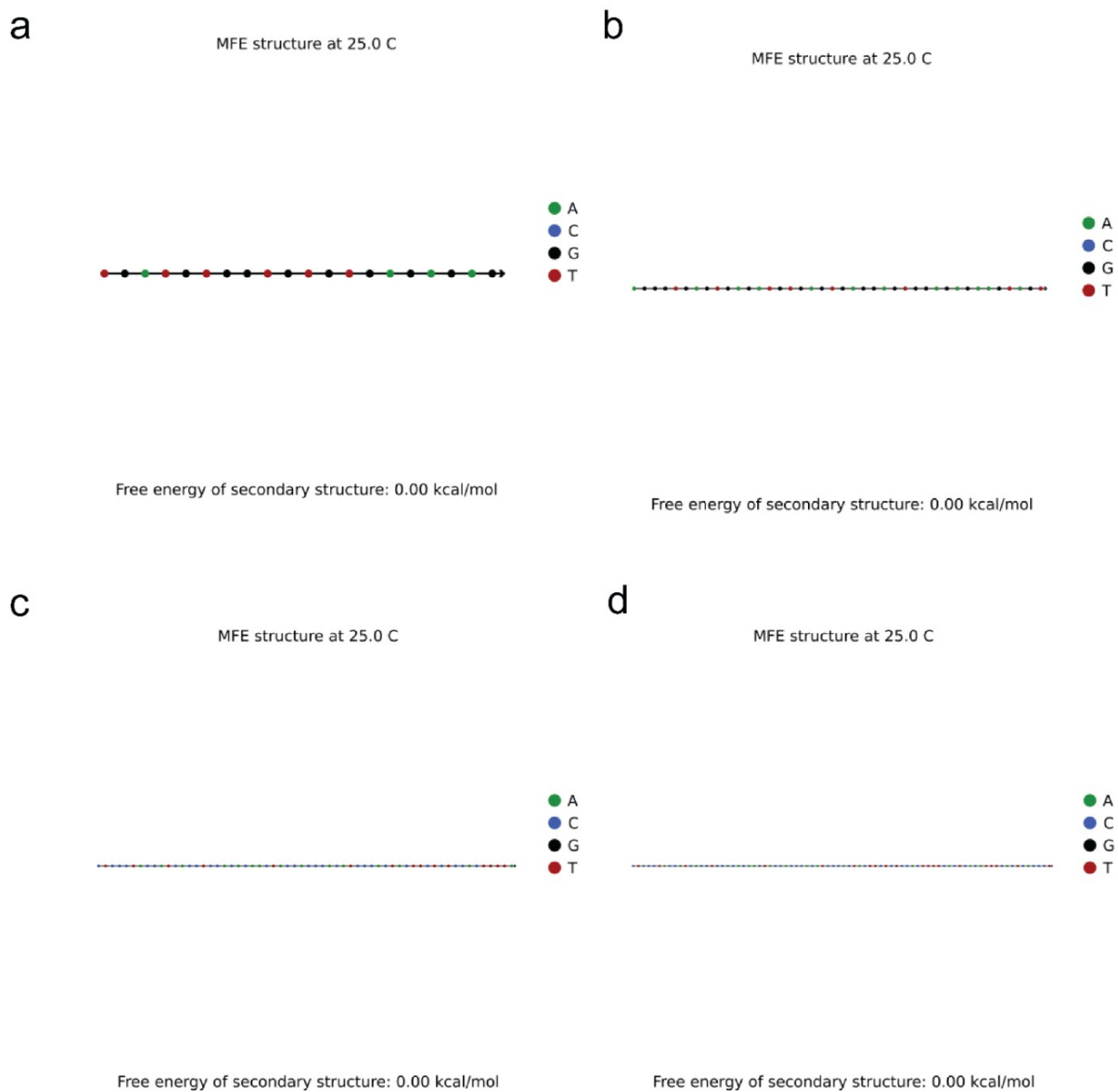


Figure S1. Thermodynamic prediction of the secondary structure of the 20 nt (a), 40 nt (b), 60 nt (c) and 80 nt (d) DNA strands used in this study. A NUPACK software was used here. These sequences were designed with 50%GC content and without secondary structure to minimize nonspecific interactions.

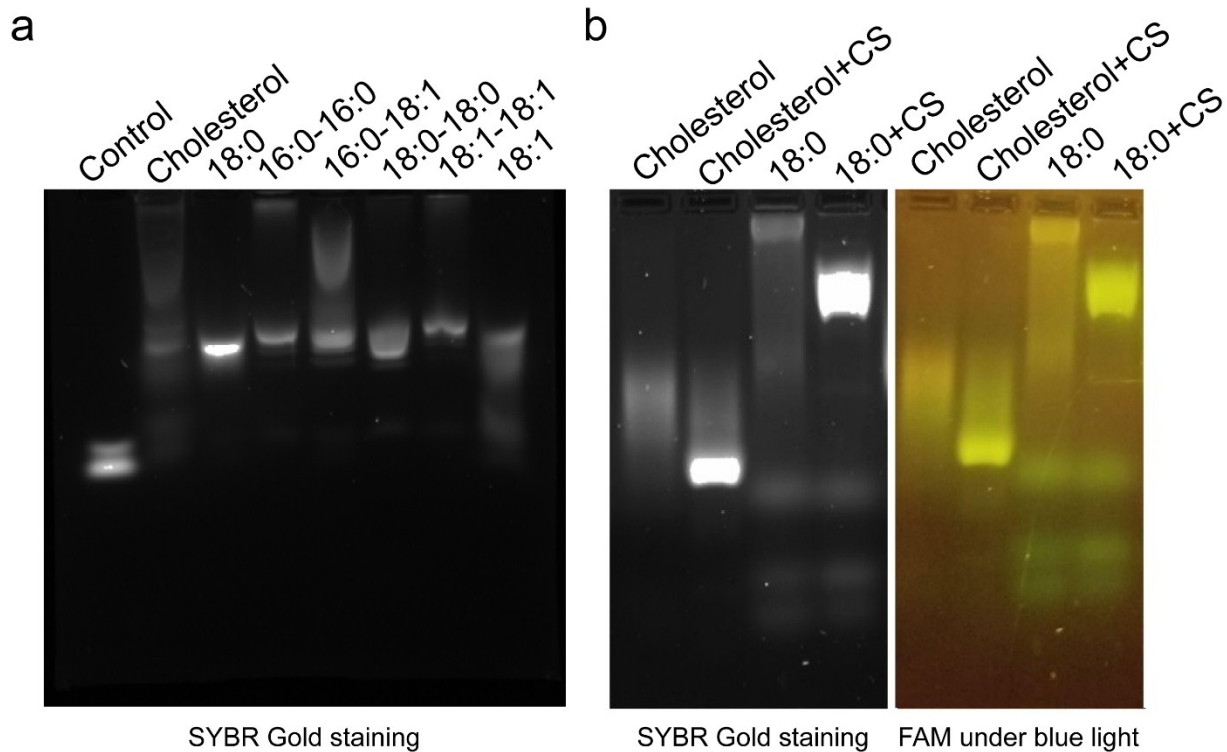


Figure S2. (a) 2% agarose gel electrophoresis for the characterization of lipid-modified 20 nt DNA. Control is the same DNA strand without lipid modification. (b) The band shift after the addition of the complementary strand (CS). Interestingly, the band migrated faster after adding the complementary strand as shown in both SYBR Gold and FAM channels. It is worth mentioning that these samples have been HPLC purified before running the gel. The observed multiple bands and smearing are believed to be due to the aggregation of lipid-DNA conjugates with different sizes or shapes.

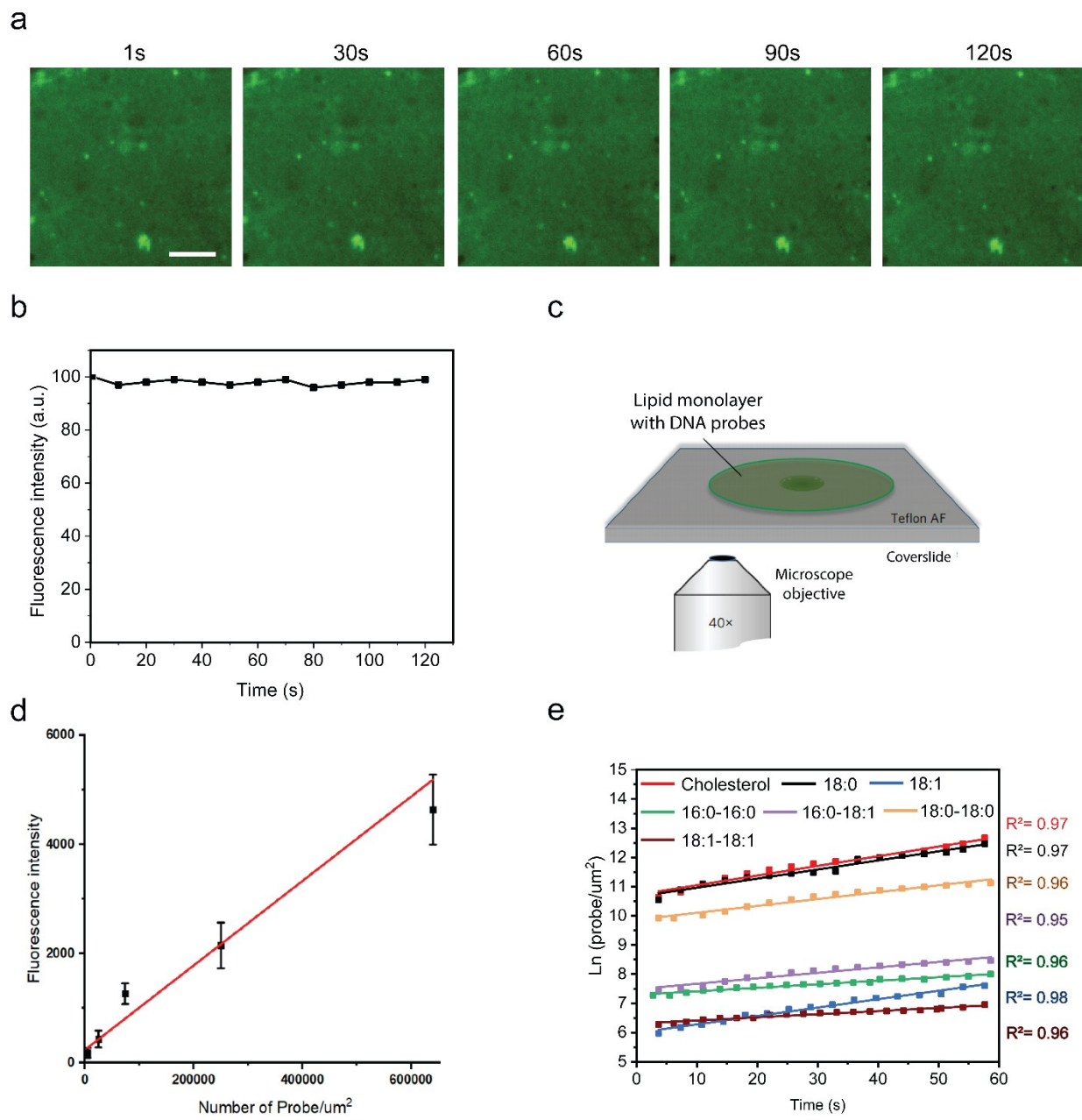


Figure S3. (a) cholesterol-DNA probe-incorporated lipid monolayer was imaged with a spinning-disk confocal microscope using the same imaging parameter as that for cellular studies, 22% laser power and 200 ms exposure time. Scale bar, 20 μm . (b) Minimal photobleaching was observed when several imaging cycles were performed on these artificial membranes. (c) Illustration of a lipid monolayer set-up on a confocal microscope to calibrate lipid-DNA probes. (d) A calibration curve to correlate the fluorescence signal intensity with the probe density within the lipid monolayer. (e) All the tested probes inserted onto the MDCK cell membranes following a first-order reaction model.

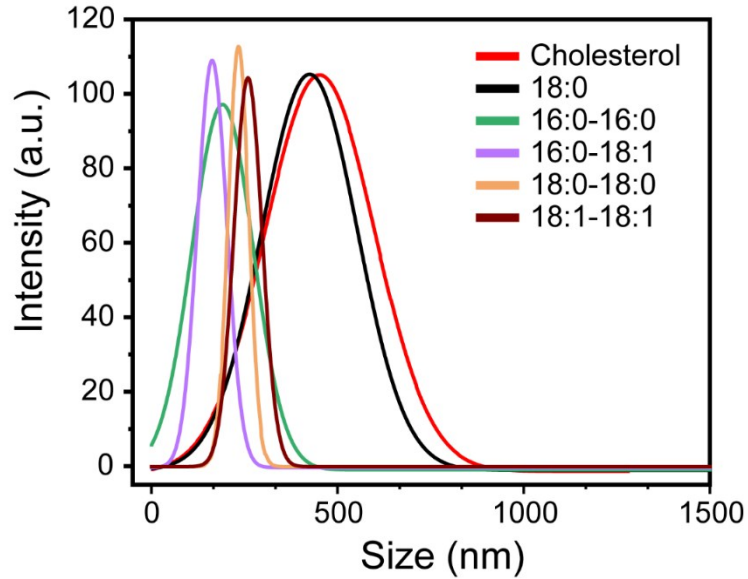
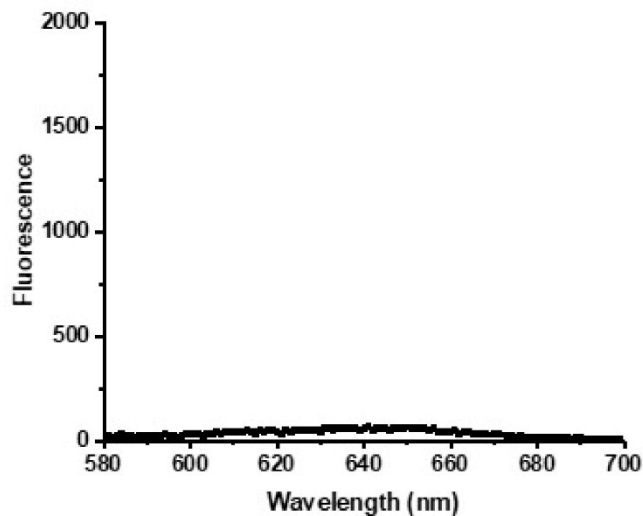


Figure S4. Size distribution of 1 μM each lipid-modified 20 nt DNA probe in HEPES buffer as measured by the dynamic light scattering. The sizes of the aggregates varied corresponding with the hydrophobicity of the lipid linker. Less hydrophobic cholesterol and 18:0 probes tended to form larger aggregates. Here, 18.1-modified probe did not show aggregations at 1 μM concentration.

a



b

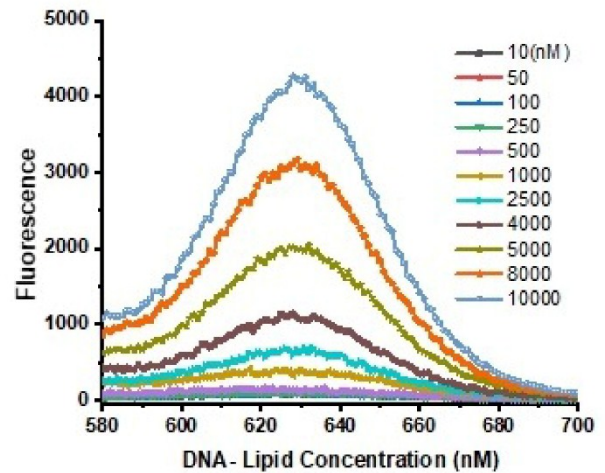


Figure S5. The fluorescence of 30 mM Nile Red in the HEPES buffer in the (a) absence or (b) presence of different concentrations of 18:0-18:0-modified 20 nt DNA probes. Here, the fluorescence increase indicated the formation of aggregates to solubilize Nile Red and prevented its precipitation.

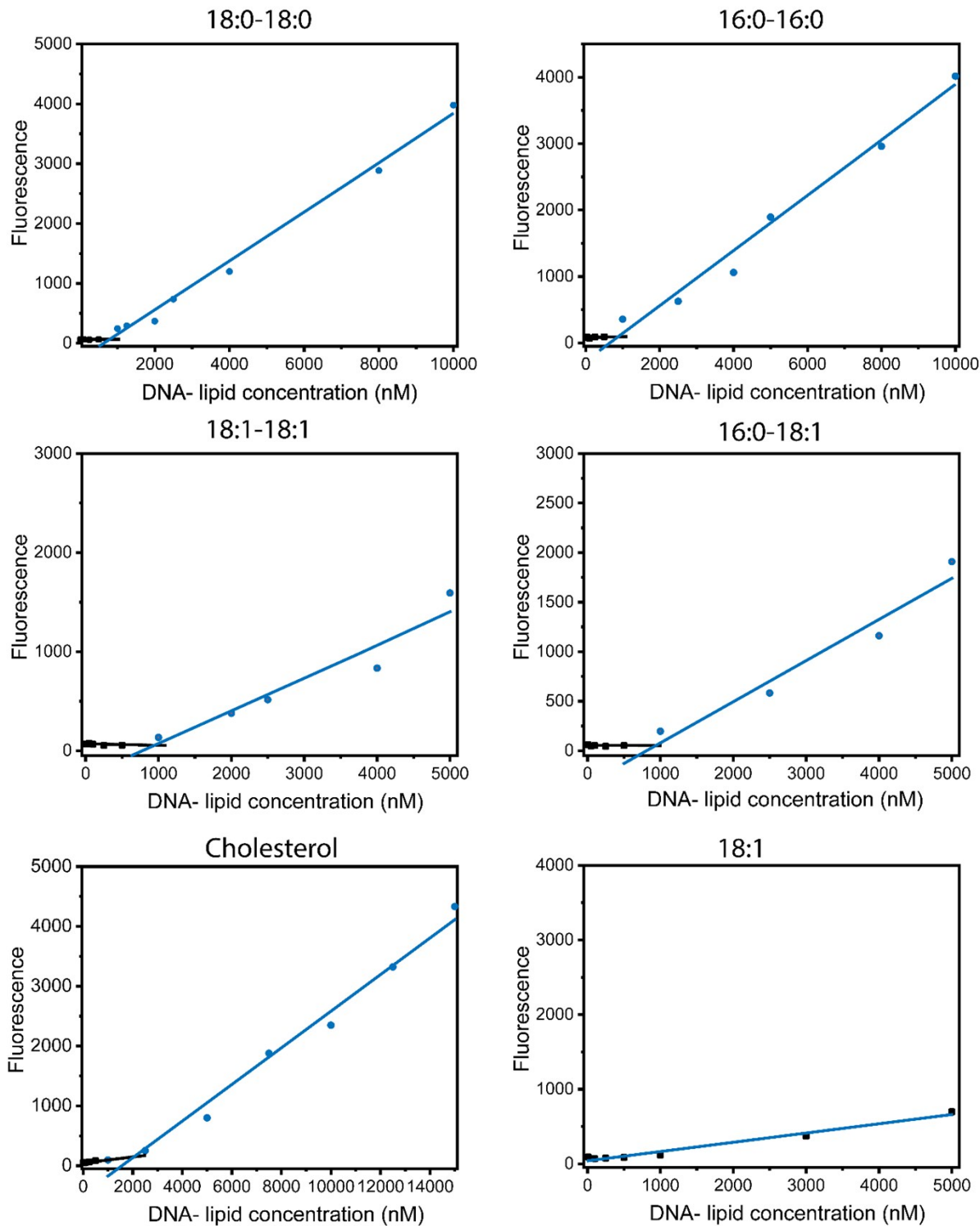


Figure S6. The critical aggregation concentration measurement as determined with the fluorescence of 30 mM Nile Red in the HEPES buffer. The intersection between two lines was used to calculate the CAC value. Similar as that shown in 18:1, we did not observe significant signal increase for 18:0-modified 20 nt DNA probe.

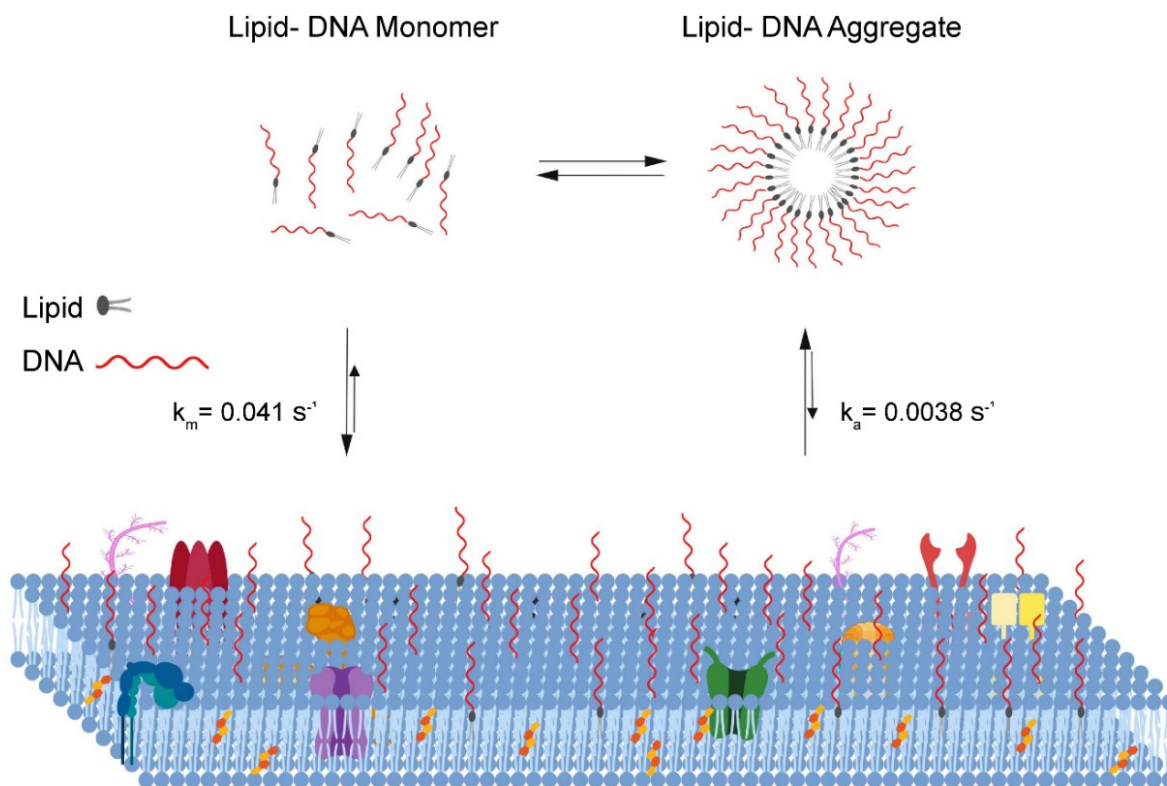


Figure S7. Schematic representation of the probe insertion into the cell membranes. Monomeric form probes could insert faster into the membranes compared to the aggregated form.

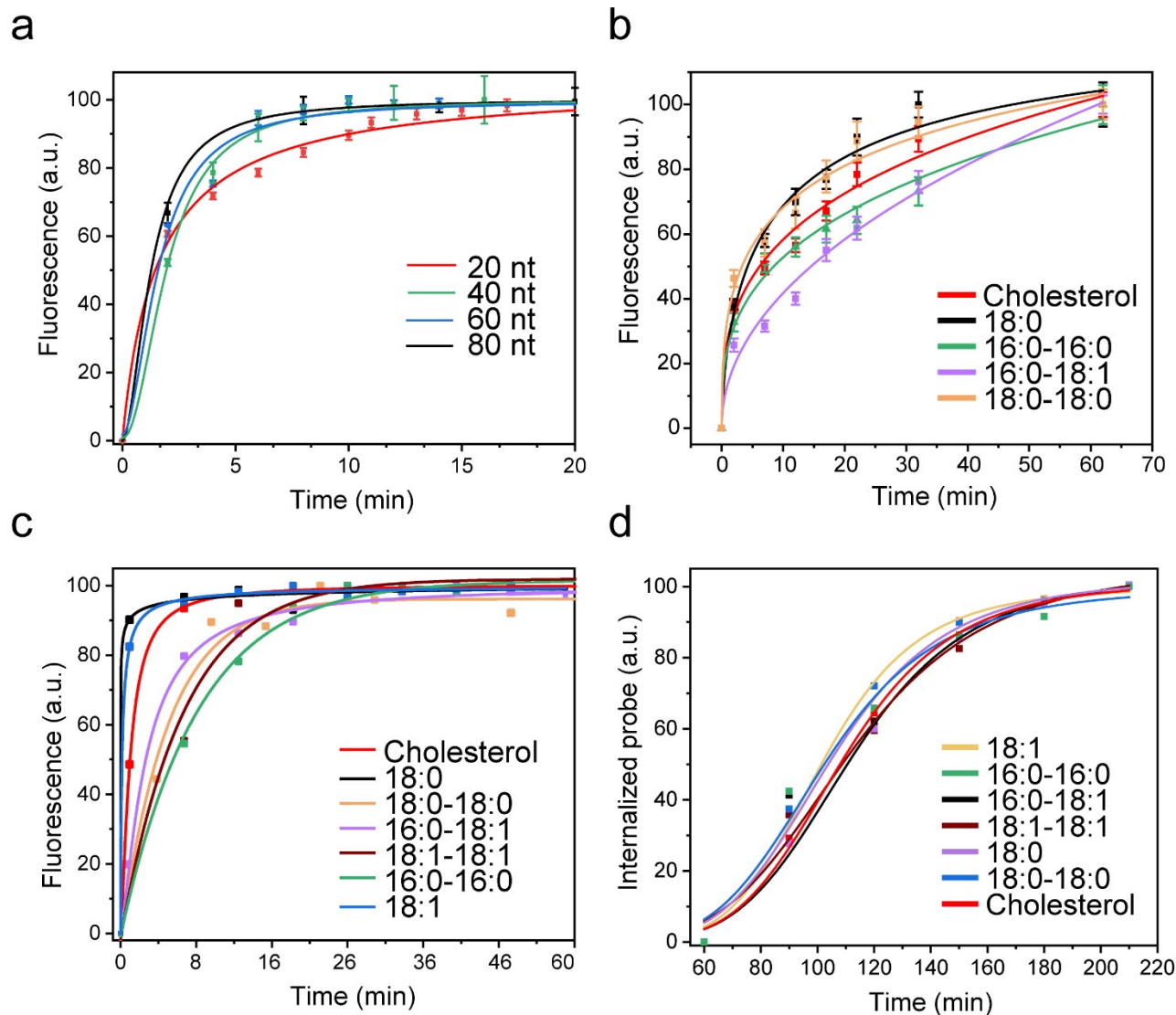


Figure S8. (a) Effect of DNA length on the probe insertion kinetics on MDCK cell membranes. 1 μM of cholesterol-modified 20 nt, 40 nt, 60 nt, and 80 nt DNA probe was added at 0 min. (b) Effect of double-stranded DNA on the probe insertion kinetics on MDCK cell membranes. 1 μM of each lipid-DNA probe containing a 20-base pair-long DNA duplexes were added at 0 min. (c) The measurement of probe insertion kinetics at 37°C. MDCK cells were incubated with 1 μM of each lipid-modified 20 nt DNA probe. Based on a first-order reaction model, the membrane insertion rate constant for each probe was calculated to be 2 – 8 fold higher at 37°C compared to that at room temperature (Table S3). The main reason for this observation could be the higher MDCK cells membrane fluidity at elevated temperature and higher probe diffusion coefficient in the solution.^{10,11} (d) The measurement of probe internalization onto the MDCK cell at 37°C. 1 μM of each lipid-modified 20 nt DNA probe was added at 0 min, and free unbound probes were removed at 60 min.

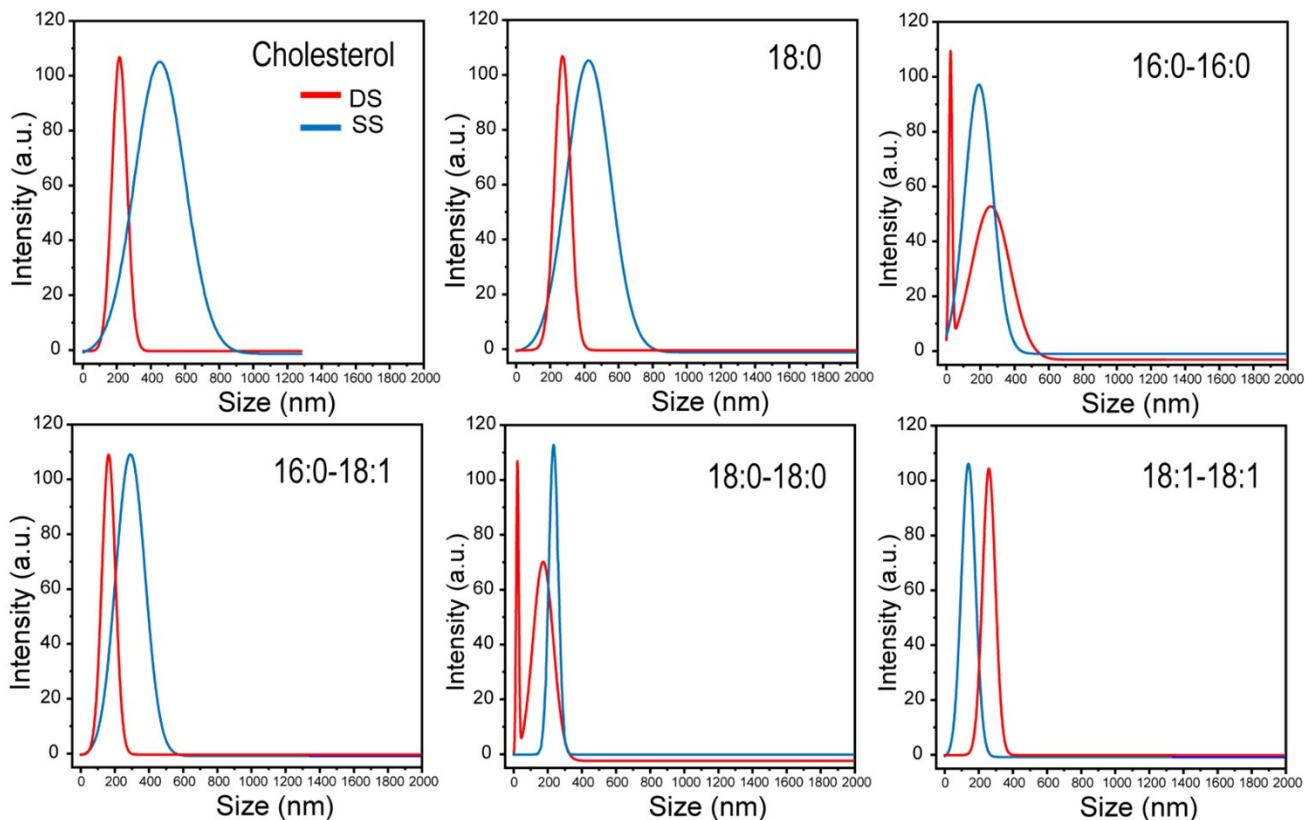


Figure S9. Effect of double-stranded 20 base pair DNA (DS, red) on the aggregation status of the lipid-DNA probes. Compared to single-stranded 20 nt DNA (SS, blue)-based probes, the addition of the complementary strands generally reduced the size of aggregates, except for 18:1-18:1.

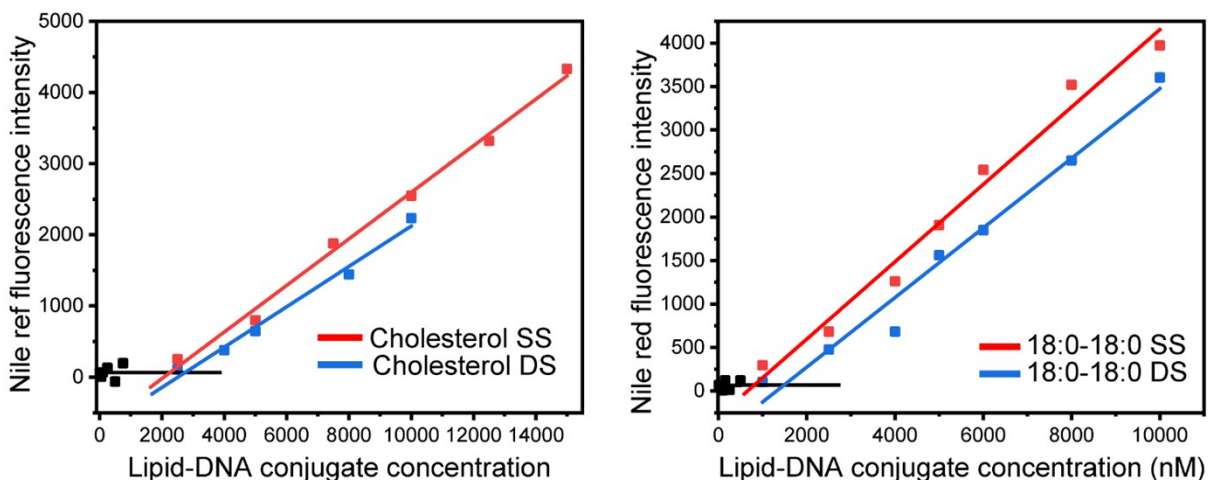


Figure S10. Effect of double-stranded (DS) DNA on the CAC values of the lipid-DNA probes. Here, a 20 nt complementary DNA was added into a single-stranded (SS) cholesterol- or 18:0-18:0-modified 20 nt DNA probe. The fluorescence of 30 mM Nile Red was measured in the HEPES buffer.

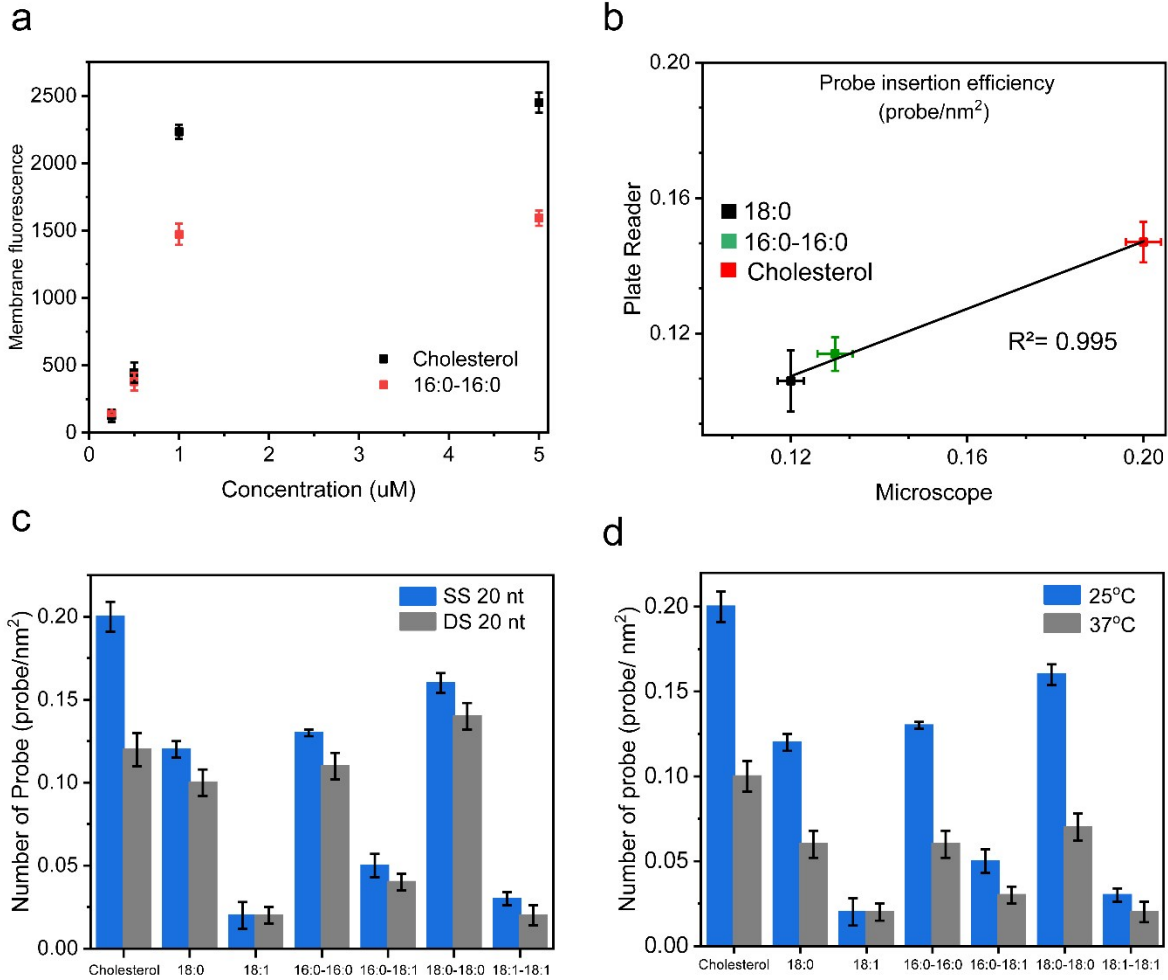


Figure S11. (a) The effect of initial probe concentration on the probe insertion efficiency into the MDCK cell membranes after 1 h incubation. (b) The probe's membrane insertion efficiency was measured by both spinning disk microscope and plate reader. In our plate reader-based assay, membrane insertion efficiency was quantified based on measuring the supernatant fluorescence intensities. Here, MDCK cells (51 K) were incubated with 100 μl of 1 μM probe for 1 h and then supernatant was separated, filtered and centrifuged to remove cell debris. The fluorescence intensity of the supernatant was measured with a Cytation 3 Cell Imaging Multi-Mode Reader (BioTek), and this data was further compared to that of reference probes of known concentrations. The probe membrane insertion density was then calculated based on the fluorescence loss in the solution and the total number and estimated surface area of cells. Shown are mean and SEM value from three experimental replicates. (c) The effect of DNA structures, double-stranded (DS) vs. single-stranded (SS), on the probe insertion efficiency on MDCK cell membrane at room temperature. (d) The effect of temperature on the probe insertion efficiency into the MDCK cell membranes after adding 1 μM each lipid-modified 20 nt DNA probe.

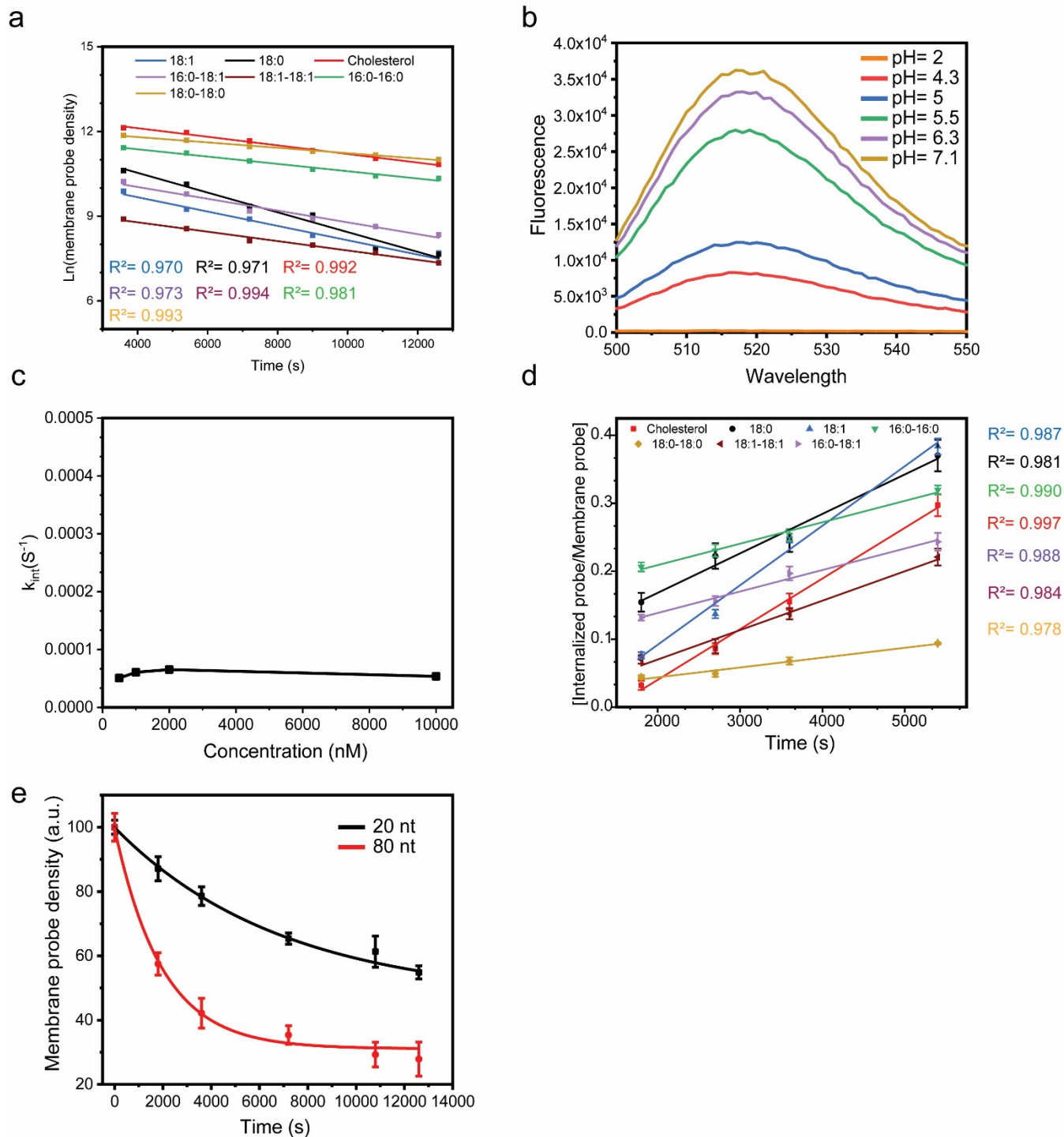


Figure S12. (a) The membrane probe density decay as measured on MDCK cell membrane follows a first-order reaction model. (b) Effect of solution pH on the 6-Fluorescein (FAM) fluorescence signal. As the pH decreased, the FAM signal was also obviously reduced. (c) Effect of initial cholesterol-DNA probe concentration on its internalization rate constant. The probe internalization rate constant is independent on its solution concentration, which suggests a first-order internalization reaction model. (d) Time-dependent change in the ratio of internalized probe vs. membrane probe is used to calculate

the initial internalization rate constant. Here, 30 min after probe modification on the cell membrane was used for the rate constant measurement, since the membrane probe concentration is relatively stable at this time window. The rate constant can be directly obtained from the slope of the graph. (e) The effect of DNA lengths on the membrane probe decay from MDCK cells. After modifying cholesterol with a longer 80 nt DNA, the membrane probe decay rate was increased due to the reduced probe hydrophobicity.

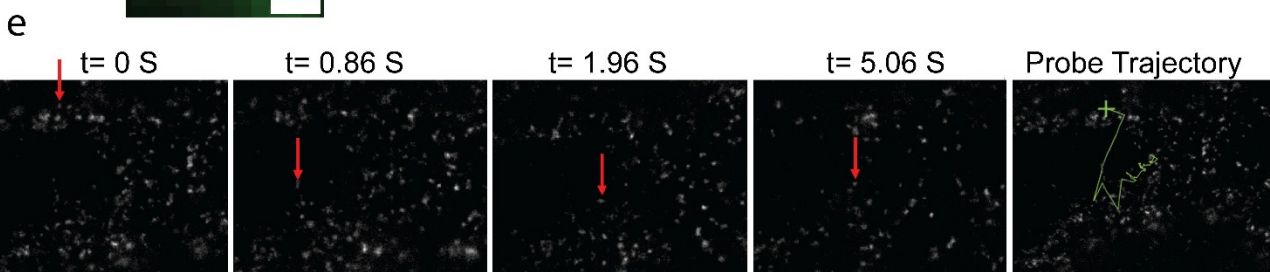
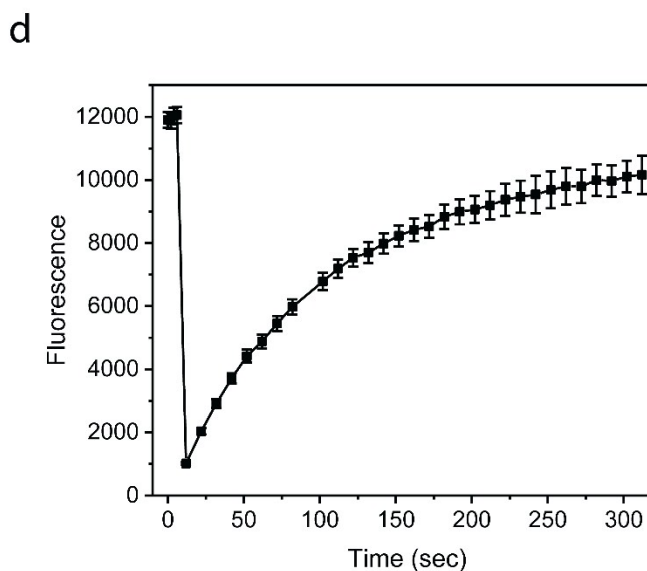
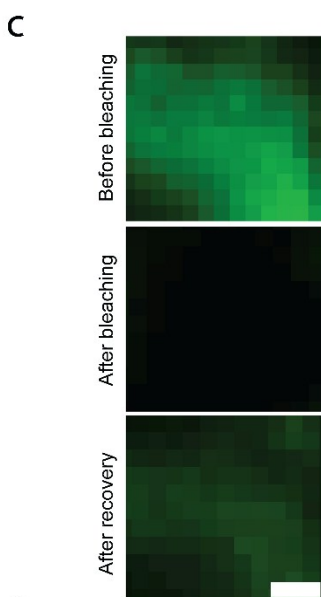
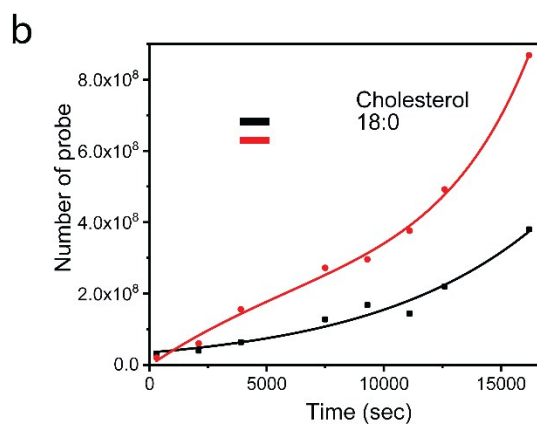
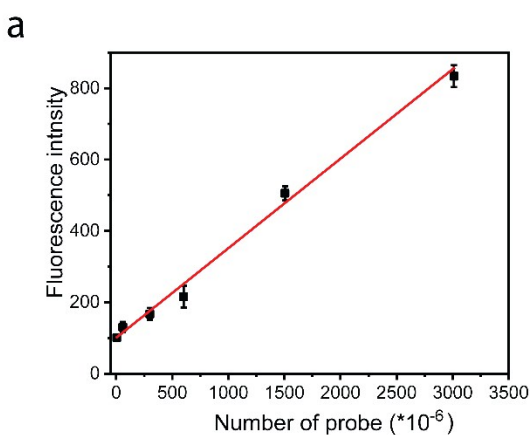


Figure S13. (a) The linear correlation between the solution fluorescence intensity and the number of lipid-DNA probes as measured by a plate reader. (b) Monitoring the cell membrane probe out-diffusion kinetics as measured based on the solution fluorescence with cholesterol- and 18.0-modified 20 nt DNA probes. (c) A representative MDCK cell membrane image was shown with cholesterol-DNA probes before the photobleaching, right after photobleaching, and after 4 min recovery. Photobleaching was performed on a circular area of interest with diameter of 2–3 μm with 50% laser power at 408 nm for 1 s and recovery was monitored for 4 min. Scale bar, 250 nm. (d) The analysis of fluorescence signal change during the FRAP process. Shown are the illustration of the fluorescence recovery curve for a cholesterol-DNA probe on MDCK cell membrane. A total of 10–20 regions of interest were bleached for each probe on the cell membrane. Similar recovery curves were obtained and averaged to measure the lateral diffusion coefficient. (e) Representative time-lapse image series of a probe diffusion among two neighboring HeLa cell membranes. Image analysis and trajectory construction were performed using an NIS-Elements software. A video illustrated this dynamic progress was also shown in the supporting information.

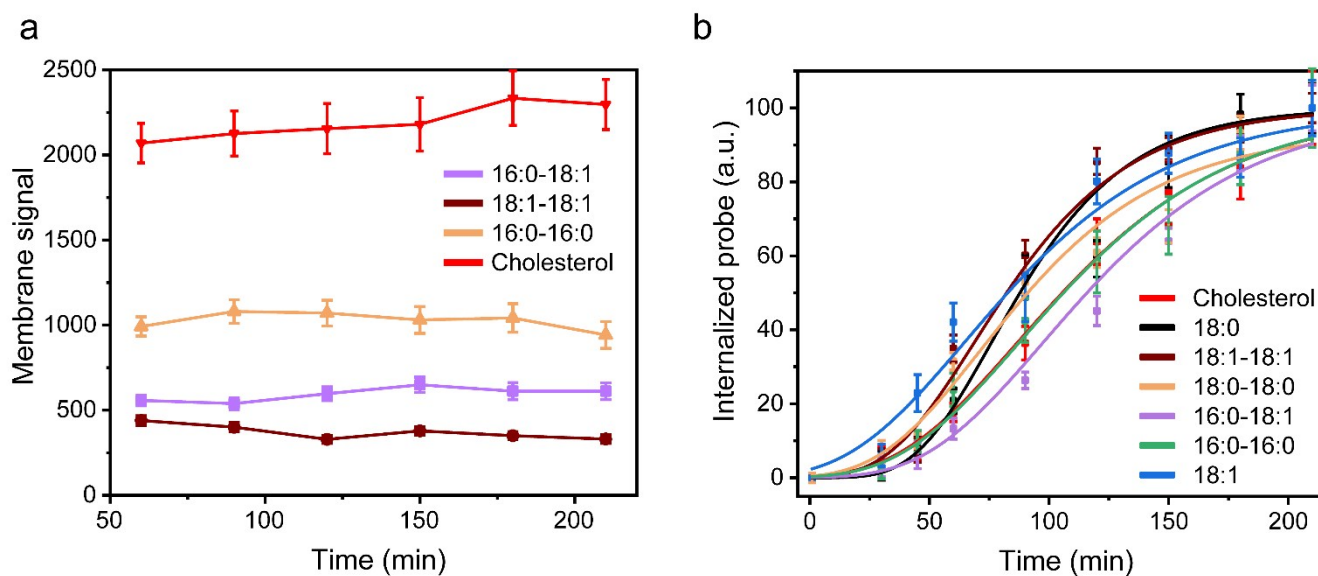


Figure S14. MDCK cell membrane signal change in the presence of excess probes in the solution. (a) 1 μM of each lipid-modified 20 nt DNA probe was added initially at 0 min. (b) During the same period, lipid-DNA probes were continuously internalized into the MDCK cells.

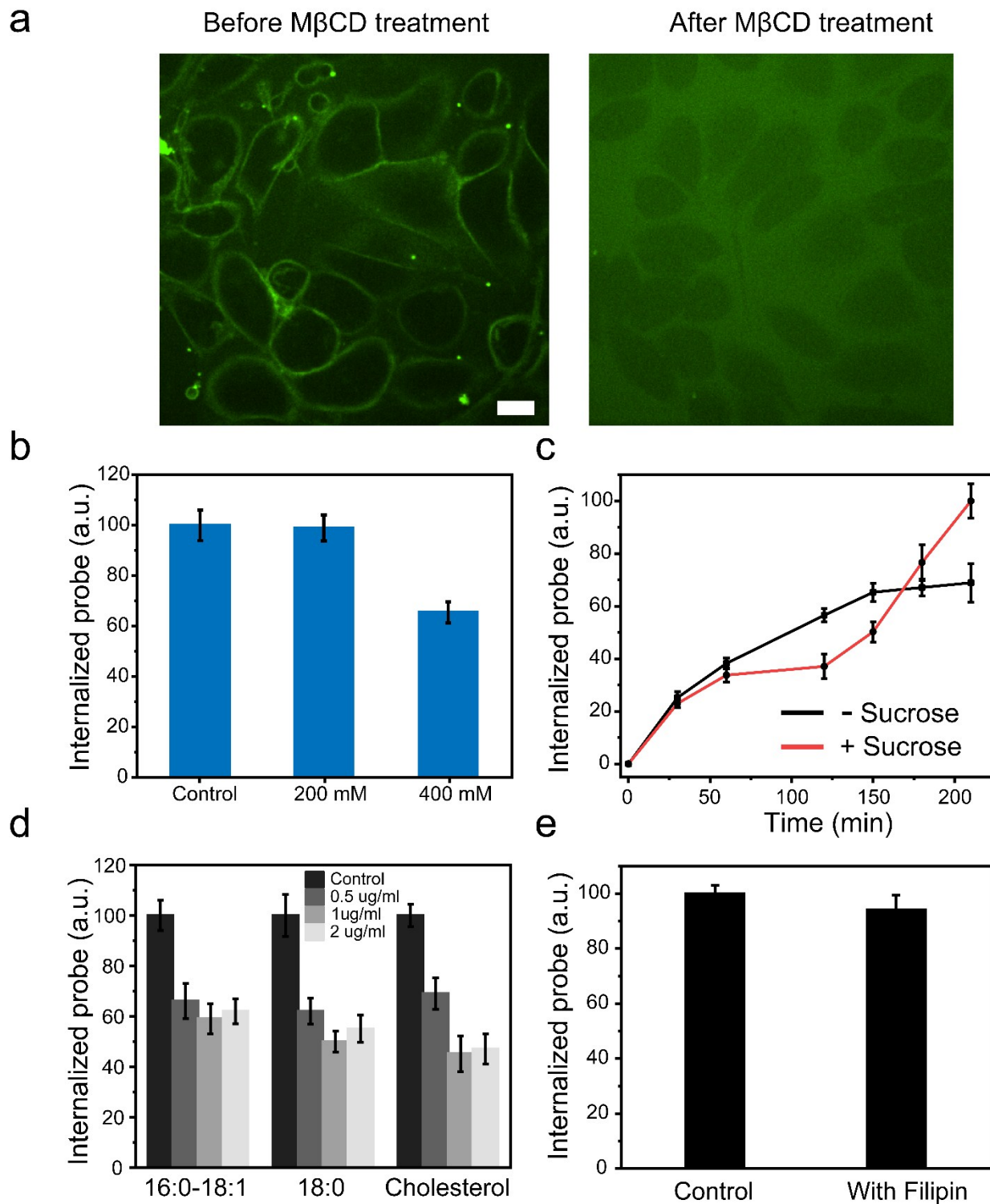


Figure S15. The effect of M β CD addition on the cell membrane modification of the probes. Shown are the MDCK cell fluorescence signal after adding 1 μ M 18:0-DNA probe for 1 h, before and 5 min after adding 5 mg/mL M β CD. Scale bar, 100 μ m. (b) The effect of sucrose concentration on the cellular

internalization of the cholesterol-DNA probe after 2 h incubation. 600 mM concentration was also tested, but obvious cell deformations were observed. (c) The internalization kinetics of the cholesterol-DNA probe in the absence or presence of 400 mM sucrose. (d) The effect of filipin concentration on the probe internalization after 2 h incubation with each lipid-DNA probe. (e) Cell membrane fluorescence signal as measured with the cholesterol-DNA probe in the presence or absence of 0.5 $\mu\text{g}/\text{mL}$ filipin for 2 h.

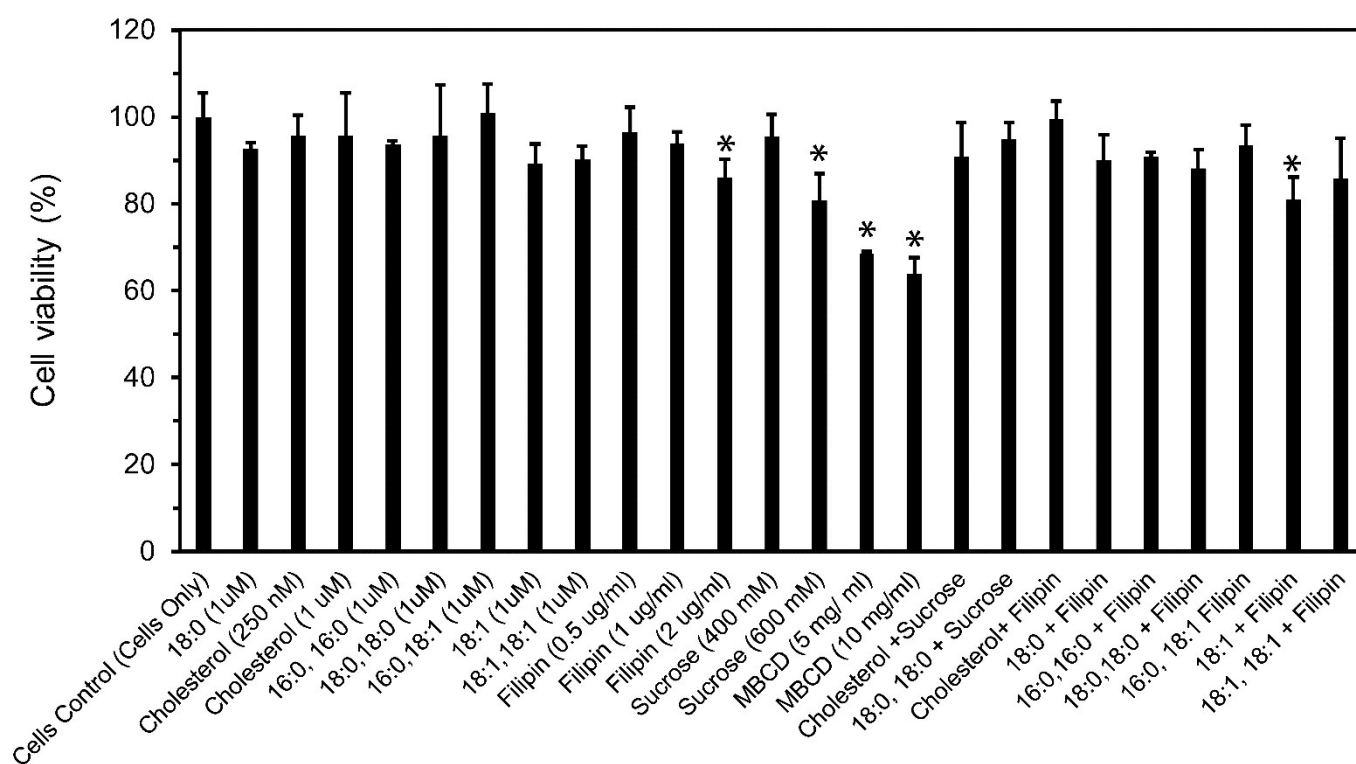


Figure S16. Alamar blue test was used to determine the MDCK cell viability after incubating with different probes and inhibitors for 4 h. The addition of lipid-DNA probes did not induce significant cytotoxicity at the tested concentrations. We observed cellular toxicity from the M β CD samples. High concentration of sucrose (>600 mM) was found to be toxic to the MDCK cells after 4 h of incubation.

REFERENCES

- 1 H. Liu, Z. Zhu, H. Kang, Y. Wu, K. Sefan and W. Tan, *Chem. - A Eur. J.*, 2010, **16**, 3791–3797.
- 2 K. Namjesnik-Dejanovic and S. E. Cabaniss, *Environ. Sci. Technol.* 2004, **38**, 1108-1114.
- 3 K. Valkó, C. Bevan and D. Reynolds, *Anal. Chem.* 1997, **69**, 2022-2029.
- 4 M. You, Y. Lyu, D. Han, L. Qiu, Q. Liu, T. Chen, C. Sam Wu, L. Peng, L. Zhang, G. Bao and W. Tan, *Nat. Nanotechnol.*, 2017, **12**, 453–459.
- 5 J. K. Hannestad, R. Brune, I. Czolkos, A. Jesorka, A. H. El-Sagheer, T. Brown, B. Albinsson and O. Orwar, *ACS Nano*, 2013, **7**, 308–315.
- 6 H. S. Wiley and D. D. Cunningham, *J. Biol. Chem.*, 1982, **257**, 4222–9.
- 7 H. S. Wiley and D. D. Cunningham, *Cell*, 1981, **25**, 433–440.
- 8 A. Salvati, C. Åberg, T. dos Santos, J. Varela, P. Pinto, I. Lynch and K. A. Dawson, *Nanomedicine Nanotechnology, Biol. Med.*, 2011, **7**, 818–826.
- 9 K. D. Lee, S. Nir and D. Papahadjopoulos, *Biochemistry*, 1993, **32**, 889–899.
- 10 Z. Mamdouh, M.-C. Giocondi, R. Laprade and C. Le Grimellec, *Biochim. Biophys. Acta - Biomembr.*, 1996, **1282**, 171–173.
- 11 M.-C. Giocondi and C. Le Grimellec, *Biochem. Biophys. Res. Commun.*, 1989, **162**, 1004–1009.